Mathematical Modeling of Axoneme Mechanics and Fluid Dynamics in Ciliary and Sperm Motility

Robert H. Dillon[1], Lisa J. Fauci[2], and Charlotte Omoto[3]
[1] Department of Mathematics
Washington State University, Pullman, WA 99164
dillon@math.wsu.edu
[2] Department of Mathematics
Tulane University, New Orleans, LA 70118
ljf@math.tulane.edu
[3] School of Biological Sciences
Washington State University, Pullman, WA 99164
omoto@wsu.edu

Abstract.
We present a fluid-mechanical model of an individual cilium or flagellum, which incorporates discrete representations of the dynein arms, and the passive elastic structure of the axoneme including the microtubules and nexin links. This model, based upon Peskin's immersed boundary method, couples the internal force generation of the molecular motors through the passive elastic structure with the external fluid mechanics governed by the Navier-Stokes equations. The flagellar and ciliary beats are not preset, but are an emergent property of the interacting components of the coupled fluid-axoneme system. The ciliary and flagellar waveforms are controlled by curvature-control mechanisms. We present numerical simulations of a ciliary beat and spermatozoa swimming.

Keywords. immersed boundary method, fluid-structure interaction, axoneme, dynein, cilia, flagella
AMS (MOS) subject classification: 92, 65, 76

1 Introduction

The eukaryotic flagella and cilia are cellular organelles that propel cells through an aqueous environment or cause fluid or mucous flow over cells. They are chemomechanical in that they convert the chemical energy of ATP into movement. They do this by the activity of dynein ATPases that produce shear forces along microtubules that form the cylindrical structures of cilia and flagella. These microtubule structures are called axonemes. The typical 9+2 arrangement, as shown in Figure 1, is a cylinder comprised of 9 doublet microtubules surrounding a pair of singlet microtubules. The doublet microtubules anchor one end of dynein, the structural attachment, while the other end of the dynein complex interacts cyclically with adjacent doublet microtubules to produce shear or sliding force. In addition to the dyneins, radial spokes attach to the peripheral doublet microtubules and span the space toward the central pair of microtubules. The radial spokes and central tubule complex are involved in the regulation of activity necessary in producing effective motion [12]. The capacity for bend propagation might rely on the effect of curvature on active sliding. Self-oscillatory behavior is an intrinsic property of the axoneme. Axonemes detached from the cell beat in

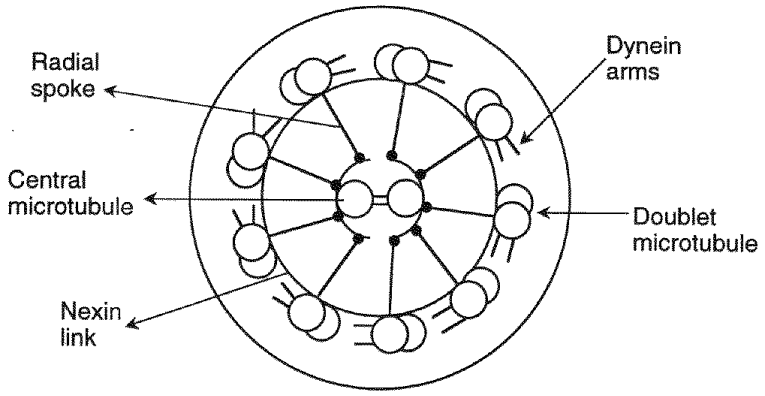

Figure 1: Diagram of the "9 + 2" axoneme.

a normal manner given appropriate ionic conditions and ATP. The typical 9+2 axoneme is found in a wide variety of protozoa, fungi, animals and lower plants. The axonemes from these divergent organisms share ultrastructural, genetic, and biochemical properties.

The bending of the axoneme is caused by sliding between pairs of outer doublets, and resistance to that sliding. Active sliding is due to the unidirectional ATP-induced force generation of the dynein power stroke. Backward, passive sliding is due to the active sliding of other pairs of doublets within the axoneme. The precise nature of the spatial and temporal control mechanisms regulating the various flagellar and ciliary beats is still unknown.

The analysis of axonemal motion began as early as the first electron micrographs showed the basic 9+2 cross-sectional images of axonemes. Gray proposed that propagation of bending waves involved the passing of active processes along the axoneme [13]. Machin used analysis of the waveform to show that the movement must arise from active elements along the whole

length of the flagellum rather than a passive elastic element driven active process at the base [24]. By recognizing that the active force is that of shear or sliding, Brokaw proposed a sliding filament model in which the curvature controls the shear force [2]. Modeling by Brokaw and by Hines and Blum in the 1970's based on balance between active, viscous and elastic moments showed that bend propagation can be explained by curvature control [3, 19]. That is, once a bend is formed, it propagates using only local curvature control. Furthermore, the curvature-control mechanism in the model can be represented as a linear function or as a simple on/off control mechanism. Both mechanisms produced waveforms observed in nature. Linear control produced a waveform resembling a sine curve, while on/off control produced a waveform resembling circular arcs connected by straight lines.

The coupled system of a viscous, incompressible fluid and a single, force-generating organism is difficult to analyze. In the past decades, the efforts to describe quantitatively the fluid dynamics of spermatozoa and ciliary propulsion have been very successful. Since the Reynolds number is quite small and inertial effects can be neglected, the linear Stokes flow assumption has been used to investigate the hydrodynamic consequences of flagellar undulations [1]. These investigations have been both analytical and computational. Resistive-force theory, initially developed by Gray and Hancock [13], makes use of the linear Stokes flow assumption, and constructs the flow field by means of distributions of fundamental singularities. Models for ciliary and flagellar motion based on a generalized resistive force theory have been developed and explored by several researchers (for example, see [3, 4, 19, 20]). A comprehensive review of this class of mathematical models is presented in [25]. Lighthill improved this theory by incorporating slender body approximations [21], since the diameter of a flagellum is much smaller than its length. More detailed hydrodynamic analysis, such as refined slender body theory and boundary element methods, have produced excellent simulations of both two- and three-dimensional flagellar propulsion in an infinite fluid domain or in a domain with a fixed wall [17, 18, 16, 31]. In all of these fluid dynamical models, the shape of the ciliary or flagellar beat was taken as given.

A model of ciliary beating that does include both internal bend-generating mechanics and accurate fluid dynamics has been developed in [14]. In this work, digitized data from the beat pattern of a cilium of a *Paramecium* has been used to calculate the parameters of an internal engine that depends only upon the geometry of the cilium. This engine is used to generate force and is coupled to a hydrodynamic model. Realistic beat patterns emerge, and metachronism is exhibited in arrays of cilia [15]. In this model, the cilium is treated as a slender body, and there is no attempt to track the individual protein structures of the axoneme.

Another model of axonemal mechanics is Lindemann's *geometric clutch* hypothesis [22, 23]. This model treats the axoneme as dynamic elastic linkages exerting force between longitudinal arrays of microtubules. The hypoth-

esis contends that the transverse force that develops in the plane of bending changes the spacing between doublet microtubules and, in turn, affects the likelihood of dynein bridges forming to pull the microtubules even closer together. The computer simulations based upon this hypothesis have produced both ciliary and flagellar waveforms. However, only a rudimentary account of the hydrodynamics is included.

In this paper we present a two-dimensional model of the fluid-axoneme system which incorporates discrete representations of the dynein arms, the passive elastic structure of the axoneme including the microtubules and nexin links. This model, based upon the immersed boundary method [27], couples the internal force generation of the molecular motors through the passive elastic structure with the external fluid mechanics. This model is an extension of our model for a single cilium which is described in [5] hereafter referred to as (I). Detailed geometric information is available, such as the spacing and shear between the microtubules, the local curvature of individual microtubules and the stretching of the nexin links. In addition, the explicit representation of the dynein motors allows us the flexibility to incorporate a variety of activation theories. Here, we choose a simple activation mechanism so that the ciliary or flagellar beat is not preset, but is an emergent property of the interacting components of the coupled fluid-axoneme system. The mathematical framework is presented in Section 2, and an outline of the numerical implementation is presented in Section 3. In Section 4, we present computational results for a curvature controlled ciliary beat, and a swimming spermatozoa with dynein kinetics governed by a curvature-control mechanism with time delay.

2 Mathematical Model

The formulation of our model is based on the immersed boundary method, first introduced by Peskin [27, 30] to model blood flow in the heart. This method treats neutrally-buoyant elastic boundaries immersed in a fluid as regions of fluid in which additional forces are applied. The immersed boundary method has been used in a variety of biological applications including the study of sperm motility in the reproductive tract [10], platelet aggregation [11], biofilm processes [6, 8], three-dimensional blood flow in the heart [28, 29], limb development [7], and large deformation of red blood cells [9].

The structure of the two-dimensional model axoneme consists of two microtubules (see Figure 2). Each microtubule is modeled as a pair of filaments with diagonal cross-links. The filaments are highly resistant to stretching and compression but offer no resistance to bending. Resistance to bending of the microtubules is governed by the elastic properties of the diagonal cross-links. Adjacent pairs of microtubules are interconnected by linear elastic springs representing the nexin and/or radial links of the axoneme. Dynein motors are represented as dynamic diagonal elastic links between adjacent pairs of

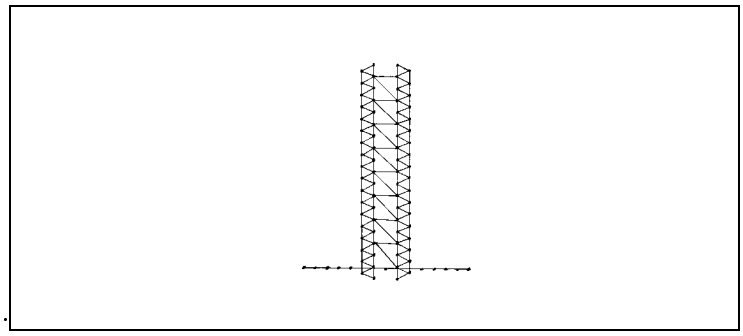

Figure 2: Schematic of model cilia in LR configuration. Each of the model axoneme's two microtubules consists of two filaments with diagonal crosslinks. The microtubules are interconnected with horizontal links representing nexins and/or radial links. The dyneins are represented as diagonal links connecting the two microtubules.

microtubules.

In cilia and flagella, the active sliding between adjacent pairs of microtubules can occur in only one direction. Thus, dyneins on different pairs of microtubules must be activated in order to produce a ciliary or flagellar beat. We accomplish this in our model by allowing *two* families of dyneins to act between the two microtubules.. The *left to right* dynein family is shown in the schematic, designated *LR family*. These dyneins are permanently attached to fixed nodes on the left microtubule. Dynein attachment on the opposite microtubule attachment sites can be transitory. Contraction of the dynein generates sliding between the two microtubules with the right hand microtubule moving upwards relative to the left. In the *right to left* family of dyneins (designated *RL family*), the dyneins are permanently attached to fixed nodes on the right hand microtubule and extend downward toward transitory attachment sites on the left hand microtubule. In either configuration, one end of a dynein can attach, detach, and reattach to attachment sites on the microtubule.

Each family of dyneins shares the space between microtubules. However, in a ciliary beat, only one family is activated during the power stroke, and the other during a recovery stroke. In a flagellar beat, the LR and RL families of dyneins are activated alternately along the length of the flagellum. The rules for activation in both the ciliary and flagellar model are discussed below. Additional immersed boundaries representing a cell wall or an entire cell body can be included. The entire structure is embedded in a viscous incompressible fluid.

2.1 Mathematical Framework

We assume that the fluid flow is governed by the Navier-Stokes equations

$$\rho\left[\frac{\partial \mathbf{u}}{\partial t} + \mathbf{u}\cdot\nabla\mathbf{u}\right] = -\nabla p + \mu\Delta\mathbf{u} + \mathbf{F}(\mathbf{x},\mathbf{t}) \quad (1)$$

$$\nabla\cdot\mathbf{u} = 0 \quad (2)$$

which describe the balance of momentum and conservation of mass in a viscous incompressible fluid. Here ρ is the fluid density, μ is the fluid viscosity, $\mathbf{u} = (u, v)$ is the fluid velocity, p denotes the pressure, and $\mathbf{F}$ is the force density (force per unit area in two dimensions) which is exerted on the fluid by the axoneme and cell wall.

The force density $\mathbf{F}$ in eqn (1)

$$\mathbf{F} = \mathbf{F}_M + \mathbf{F}_N + \mathbf{F}_D + \mathbf{F}_C + \mathbf{F}_T \quad (3)$$

includes contributions arising from the deformation of the elastic structure of the microtubules $\mathbf{F}_M$, elongation of the nexin/radial links $\mathbf{F}_N$, contraction of the dynein links $\mathbf{F}_D$, forces that represent the cell wall (in the case of ciliary motion) or cell body (in the case of flagellar motion) $\mathbf{F}_C$, and tethering forces that attach the axoneme to a cell wall or a cell body.

Each of the microtubules, in this two-dimensional model, is represented at time t as a pair of one-dimensional filaments, $\mathbf{X}^k(s,t)$, indexed by a Lagrangian parameters s (arclength in an unstressed configuration). The force per unit length $\mathbf{f}^k(s,t)$

$$\mathbf{f}^k = \mathbf{f}^k_M + \mathbf{f}^k_N + \mathbf{f}^k_D + \mathbf{f}^k_T \quad (4)$$

along the k^{th} filament includes contributions from elastic structure of the microtubules $\mathbf{f}^k_M$, nexin/radial links, $\mathbf{f}^k_N$, dynein links $\mathbf{f}^k_D$, and tethering forces that attach the base of the axoneme to a cell wall or cell body $\mathbf{f}^k_T$. The force densities $\mathbf{F}_X$, $X = M, N, D, T$ in eqn (3) are obtained via integration

$$\mathbf{F}_X(\mathbf{x},t) = \sum_k \int \mathbf{f}^k_X(s,t)\delta(\mathbf{x} - \mathbf{X}^k(s,t))ds. \quad (5)$$

Here, the integrations are over the filaments, and δ is the two-dimensional Dirac delta function.

In addition, we impose the condition that the velocity of the microtubules and cell wall or body must be equal to the local fluid velocity at each point.

$$\frac{\partial \mathbf{X}^K(s,t)}{\partial t} = \mathbf{u}(\mathbf{X}^k(s,t),t) = \int \mathbf{u}(\mathbf{x},t)\delta(\mathbf{x} - \mathbf{X}^k(s,t))d\mathbf{x} \quad (6)$$

A detailed description of the discretized model is shown in (I). The microtubule filaments $\mathbf{X}^k(s,t)$ are discretized and represented as *immersed boundary points* or *nodes* $\mathbf{X}^k_i(t)$ with $i = 1, \ldots N_p$. Similarly, the microtubule forces

$\mathbf{f}_X^k(s,t)$ are represented as discrete forces $\mathbf{f}_{X,i}^k(t)$ at the immersed boundary points. The filaments themselves are composed of individual elastic links. The diagonal cross-links and filament links attach at the immersed boundary points. A schematic of the discrete model is shown in Figure 2.

Dyneins are represented in the model as elastic links between the two microtubules.

- **LR family**

  The active dyneins are oriented diagonally downwards from the left microtubule to the right microtubule. As these dyneins contract, the right microtubule slides distally relative to the left microtubule. If the microtubules are tethered to a fixed cell wall, as in ciliary beating, the structure bends toward the right.

- **RL family**

  The active dyneins are oriented diagonally downwards from the right microtubule to the left microtubule. As these dyneins contract, the left microtubule slides distally relative to the right microtubule. It the microtubules are tethered to a fixed cell wall, as in ciliary beating, the structure bends toward the left.

For each family, dynein connectivity is reassessed at each time step of a numerical simulation. As the microtubules slide, the endpoint of a dynein link may 'ratchet' from one node of the microtubule to another. Nexin links and or radial spokes are also represented in this model. The dynein forces and nexin/link forces in this model can also be viewed as a single mechanism describing a model dynein. The tangential forces of the diagonal links generate the shear forces and are responsible for sliding, whereas the nexin/radial link forces resist changes in intermicrotubule spacing.

The forces due to all of the springs representing the filament links, diagonal cross-links, nexin/radial spoke links, and dyneins contribute to the force density function at each of the nodes. A discrete version of eqn (3) is used to spread this force density defined along microtubules to a force field on the fluid domain. The microtubule point forces are distributed to the fluid by the use of an approximate delta function of the form $\delta_h(\mathbf{x}) = d(x)d(y)$ where h is mesh width of the finite difference fluid grid and

$$d(r) = \begin{cases} \frac{1}{4h}\left(1+\cos\frac{\pi r}{2h}\right) & \mid r \mid < 2h \\ 0 & \mid r \mid \geq 2h. \end{cases} \tag{7}$$

We refer the reader to [27] for details.

We can summarize the immersed boundary algorithm as follows: Suppose that at the end of timestep n we have the fluid velocity field $\mathbf{u}^n$ on a grid, and the configuration of the immersed boundary points comprising the filaments of the microtubules $(\mathbf{X}^k)^n$ and the cell wall or cell body $(\mathbf{X}_c)^n$. Then to advance the system by one timestep we:

1. Reassess the connectivity structure of dynein motors and nexin/radial spoke links;
2. Determine the activation state of dyneins based upon the configuration of the filaments of the microtubules $(\mathbf{X^k})^n$;
3. Calculate the force densities $\mathbf{f}^k$ from the microtubule boundary configuration, dyneins, nexins links and axonemal tethers;
4. Calculate the force densities $\mathbf{f}_c$ from the cell wall or body configuration $(\mathbf{X}_c)^n$;
5. Spread the force densities to the grid to determine the forces $\mathbf{F}$ on the fluid;
6. Solve the Navier-Stokes equations for the fluid velocities $\mathbf{u}^{n+1}$;
7. Interpolate the fluid velocity field to each immersed boundary point $(\mathbf{X}^k)^n$ and $(\mathbf{X}_c)^n$ and move the point at this local fluid velocity.

It is in step (2) that we may implement different dynein activation strategies. The kinetics of individual dynein activation may depend upon the geometry of the structure, such as local curvature, shear and intermicrotubule spacing. In addition, the activation kinetics may be stochastic. For a comprehensive discussion of the modeling of dynein activation, see [25].

The crucial feature of this fluid-structure interaction model is that the axoneme is not the computational boundary in the Navier-Stokes solver. This immersed boundary is the source of a dynamic force field which influences the fluid motion through the force term in the fluid equations. Since the computational domain is a fixed rectangle, we can use an efficient fluid solver designed for a regular grid with simple boundary conditions.

3 Numerical Simulations

In this section we present numerical results from simulations that generate a ciliary beat governed by a curvature controlled recovery mechanism, and spermatozoa motility using a curvature control mechanism with time delay. The computational parameters for the sperm simulations are similar to those used in the cilia simulations as shown in (I).

Ciliary beat

We first show results of a simulation with an asymmetrical beat featuring a power stroke in LR mode and a recovery stroke in the RL mode. We employ a *geometric switch* to determine when the cilium beat changes directions. We monitor the shear between microtubules and change the direction of the ciliary beat once the shear has exceeded a specified threshold. Once the recovery stroke is initiated, a traveling wave of dynein activation proceeds from

base to tip. The traveling wave speed is not imposed during the simulation but is controlled by a curvature-control algorithm. Throughout the recovery stroke the dynein configuration is set to the RL mode. At time t^n dyneins in the RL mode with indices less than or equal to p^n are activated, dyneins with indices greater than p^n are inactive. The algorithm for updating the index p^n is as follows. At the beginning of time step t^n, we

1. approximate the curvature κ_i, $i = 1, ..N_p$, at the location of i^{th} dynein from the configuration of the filament to which the dyneins are permanently attached;

2. determine p_{max}, the index of greatest axonemal curvature where p_{max} satisfies $\kappa_{p_{max}} = max_i\,(\kappa_i)$;

3. set $p^n = p_{max} + k$, where k is typically 3.

At the beginning of the recovery stroke, we set $p^n = max(p_{min}, p_{max})$. In the simulation shown here, we set $p_{min} = N_p/4$.

We remark that in this mechanism, the dynein activation wave front is just ahead of the point of maximum axonemal curvature. Note that the wave front does not advance unless the point of maximum curvature advances. In this mechanism, the parameter p^n marking the leading edge of the dynein activation cannot decrease. Although dynein activation extends from the cilium base to a point just beyond the point of maximum curvature, activation cannot advance until the point of maximum curvature has moved at least one node distally. The increases of p^n do not occur at regular time intervals. In fact, these time intervals are highly irregular.

In Figure 3, we show snapshots from one complete ciliary beat.

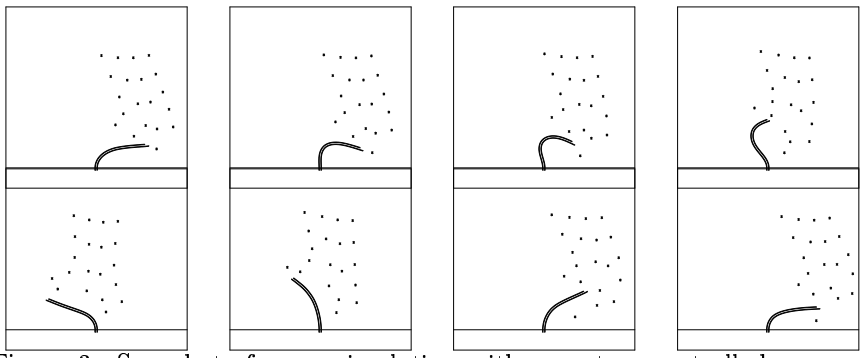

Figure 3: Snapshots from a simulation with curvature-controlled recovery stroke showing one complete beat.

Sperm motility

In this section we show numerical results from simulations of the sperm model. In these, the axonemal structure is identical to that used in the cilia simulations with the addition of a cell body attached at the base of the

axoneme. The cell body itself consists of a ring of immersed boundary points interconnected with linear elastic spring elements. These springs connect each immersed boundary point on the cell wall with the nearest and next nearest neighbors.

The flagellar waveform is governed by a simple curvature control algorithm in which individual dyneins are selected from the LR or RL families at each time step according to the local curvature at the site of the dynein at a time τ *in the past*. The choice of modes depends on the sign of the lagged local curvature. The initial shape of the axoneme has a pair of bends. Once the simulation begins, the resulting bend propagation depends only on this curvature control mechanism.

In Figures 4 and 5 we show the results of three simulations. These illustrate the effect of changing the lag time and fluid viscosity parameters. In Figure 4 we show several snapshots of the swimming sperm. As seen in panels (a) and (b), the beat frequency and swimming speeds are strongly correlated with the lag time τ. A longer lag time results in a slower beat and decreased swimming speed. The swimming speed in panel (c) is greatly reduced. This is due to the increased lag time and fluid viscosity increased 10 fold.

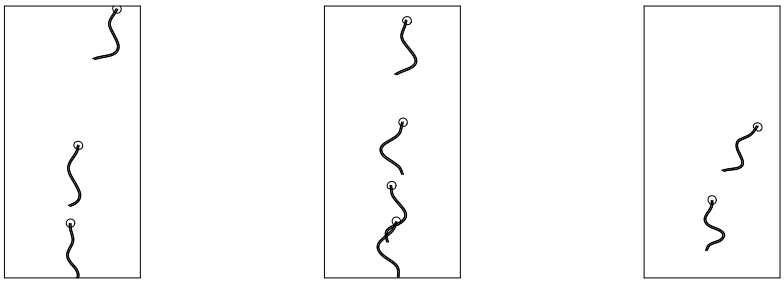

(a) (b) (c)

Figure 4: Simulations of sperm motility. Panel (a) $\nu = 1cp$, $\tau = 2$ milliseconds, beat frequency: 115 HZ, swimming speed: 500 μ/s. Panel (b) $\nu = 1cp$, $\tau = 4$ milliseconds, beat frequency: 70 HZ, swimming speed: 250 μ/s. Panal (c) $\nu = 10cp$, $\tau = 8$ milliseconds, beat frequency: 30 HZ, swimming speed: 30 μ/s.

In Figure 5, we show shear plots from each of the three simulations. The shear angle is the angle formed between the horizontal axis and the tangent line to the flagellum. Although the wavelength of the flagellar waveforms are similar in each simulation, there are significant differences in the shear angle profiles.

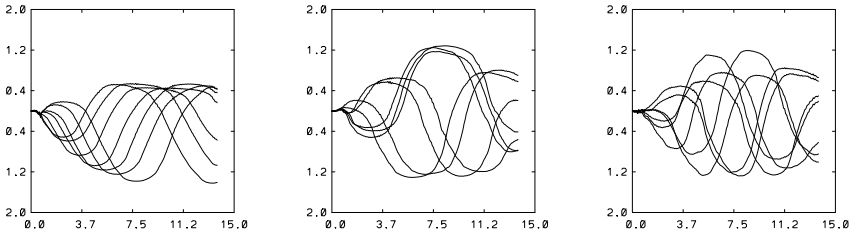

(a) (b) (c)

Figure 5: Flagellar shear plots. Length in microns x axis with shear angle in radians on the y axis.

4 Discussion

We have presented a new model based on the immersed boundary method for studying ciliary and flagellar motion. The numerical results demonstrate the feasibility of this fluid-structure interaction model to simulate both ciliary and flagellar beats. This model is robust in the sense that the axonemal structure shows no signs of degradation over many beats and gives reasonable results over a range of fluid viscosities.

Curvature-control mechanisms govern the generation of the recovery waveform in the cilium and of the flagellar beat for the sperm. There are significant differences in the description of the control mechanisms for the two types of beats. However, there is an interesting parallel between the two. Although the choice dynein type (RL or LR) in the flagellar beat at time t was determined by the local curvature at time $t - \tau$, changes along the axoneme from one dynein configuration to the other are found near points of maximum curvature at time t. Thus, it may be possible to obtain a ciliary recovery stroke via a lagged curvature-control mechanism as well. This will be explored in future work.

In the future, we will consider two general areas of development for the ciliary/flagellar motion model. The first is the obvious extension to three dimensions and we will initially present a simplified three-dimensional model with two microtubules similar to the one shown here. We plan to investigate a variety of phenomena initially with the two-dimensional model. In particular, we are constructing alternative mechanisms for controlling dynein activation that include explicit representation of geometry-dependent chemical kinetics and will consider in detail how well the various mechanisms reproduce experimental results associated with changing viscosity and ATP concentrations. There are good estimates for the various rate parameters governing the dynein enzyme kinetics for several of the multistate models (see [26] for example). The lag times used in our sperm simulations are on the order of a few milliseconds and are consistent with the characteristic time scales of

dynein kinetics. We expect that the substitution of a more realistic kinetic model for the activation of individual dyneins will lead to results similar to those shown here.

Acknowledgements

The work of the authors was supported in part by NSF grant DMS 0201063. The work of Robert Dillon was supported in part by NSF grant DMS 0109957.

References

[1] C. Brennen and H. Winet. Fluid mechanics of propulsion by cilia and flagella. *Ann. Rev. Fluid Mech.*, 9:339–398, 1977.

[2] C. J. Brokaw. Bend propagation along flagella. *Nature*, 209:161–163, 1966.

[3] C. J. Brokaw. Computer simulation of flagellar movement. I. Demonstration of stable bend propagation and bend initiation by the sliding filament model. *Biophys. J*, 12:564–586, 1972.

[4] C. J. Brokaw and D. Rintala. Computer simulation of flagellar movement. V. Oscillation of cross-bridge models with an atp-concentration-dependent rate function. *J. Mechanochem. Cell Motil.*, 4:205–227, 1977.

[5] R. Dillon and L. J. Fauci. An integrative model of internal axoneme mechanics and external fluid dynamics in ciliary beating. *J. theor. Biol.*, 207:415–430, 2000.

[6] R. Dillon, L. J. Fauci, A. Fogelson, and D. P. Gaver. Modeling biofilm processes using the immersed boundary method. *J. Comp. Phys*, 129:57–73, 1996.

[7] R. Dillon and H. G. Othmer. A mathematical model for outgrowth and spatial patterning of the vertebrate limb bud. *J. theor. Biol.*, 197:295–330, 1999.

[8] Robert Dillon and Lisa Fauci. A microscale model of bacterial and biofilm dynamics in porous media. *Biotechnol. Bioeng.*, 68:536–547, 2000.

[9] C. D. Eggleton and A. S. Popel. Large deformation of red blood cell ghosts in a simple shear flow. *Phys. Fluids*, 10:1834–1845, 1998.

[10] L. J. Fauci and A. McDonald. Sperm motility in the presence of boundaries. *Bull. Math. Biol.*, 57(5):679–699, 1995.

[11] A. L. Fogelson. A mathematical model and numerical method for studying platelet adhesion and aggregation during blood clotting. *J. Comp. Phys.*, 56:111–134, 1984.

[12] L. C. Gardner, E. O'Toole, C. A. Perrone, T. Giddings, and M. D. Porter. Components of a "dynein regulatory complex" are located at the junction between the radial spokes and the dynein arms in *chlamydomonas* flagella. *J. Cell Biol.*, 127:1311–1325, 1994.

[13] J. Gray and G. Hancock. The propulsion of sea-urchin spermatozoa. *J. Exp. Biol.*, 32:802–814, 1955.

[14] S. Gueron and K. Levit-Gurevich. Energetic considerations of ciliary beating and the advantage of metachronal coordination. *Proc. Natl. Acad. Sci. USA*, 96:12240–12245, 1999.

[15] S. Gueron, K. Levit-Gurevich, N. Liron, and J.J. Blum. Cilia internal mechanism and metachronal coordination as the result of hydrodynamic coupling. *Proc. Natl. Acad. Sci. USA*, 94:6001–6006, 1997.

[16] J.J.L. Higdon. The generation of feeding currents by flagellar motion. *J. Fluid Mech.*, 94:305–330, 1979.

[17] J.J.L. Higdon. A hydrodynamic analysis of flagellar propulsion. *J. Fluid Mech.*, 90:685–711, 1979.

[18] J.J.L. Higdon. The hydrodynamics analysis of flagellar propulsion: helical waves. *J. Fluid Mech.*, 94:331–351, 1979.

[19] M. Hines and J. J. Blum. Bend propagation in flagella. I. Derivation of equations of motion and their simulation. *Biophys. J*, 23:41–57, 1978.

[20] M. Hines and J. J. Blum. Bend propagation in flagella. II. Incorporating of dynein cross-bridge kinetics into the equations of motion. *Biophys. J*, 25:421–442, 1979.

[21] J.L. Lighthill. Flagellar hydrodynamics. *SIAM Review*, 18:161–230, 1976.

[22] C. B. Lindemann. A 'geometric clutch' hypothesis to explain oscillations of the axoneme of cilia and flagella. *J. theor. Biol.*, 168:175–189, 1994.

[23] Charles B. Lindemann. Geometric clutch model version3: The role of the inner and outer arm dyneins in the ciliary beat. *Cell Motil. Cytoskeleton*, 52:242–254, 2002.

[24] K. D. Machin. Wave propagation along flagella. *J. Exp. Biol*, 35:796–806, 1958.

[25] M. Murase. *The Dynamics of Cellular Motility.* John Wiley, Chichester, 1992.

[26] C. K. Omoto, J. S. Palmer, and M. E. Moody. Cooperativity in axonemal motion: Analysis of a four-state, two-site kinetic model. *Proc. Natl. Acad. Sci. USA*, 88:5562–5566, 1991.

[27] C. S. Peskin. Numerical analysis of blood flow in the heart. *J. Comp. Phys.*, 25:220–252, 1977.

[28] C. S. Peskin and D. M. McQueen. A three-dimensional computational model for blood flow in the heart I. immersed elastic fibers in a viscous incompressible fluid. *J. Comp. Phys*, 81:372–405, 1989.

[29] C. S. Peskin and D. M. McQueen. A three-dimensional computational model for blood flow in the heart II. *J. Comp. Phys*, 82:289–297, 1989.

[30] Charles S. Peskin. The immersed boundary method. *Acta Numerica*, pages 1–39, 2002.

[31] N. Phan-thien, T. Tran-cong, and M. Ramia. A boundary-element analysis of flagellar propulsion. *J. Fluid Mech.*, 184:533–549, 1987.